



Since January 2020 Elsevier has created a COVID-19 resource centre with free information in English and Mandarin on the novel coronavirus COVID-19. The COVID-19 resource centre is hosted on Elsevier Connect, the company's public news and information website.

Elsevier hereby grants permission to make all its COVID-19-related research that is available on the COVID-19 resource centre - including this research content - immediately available in PubMed Central and other publicly funded repositories, such as the WHO COVID database with rights for unrestricted research re-use and analyses in any form or by any means with acknowledgement of the original source. These permissions are granted for free by Elsevier for as long as the COVID-19 resource centre remains active.



Glucosamine and maltol anchored Zinc(II) complex of COVID-19 health supplement relevance: DFT collaborated spectroscopic formulation with profound biological implications

Jan Mohammad Mir^{a,b,*}, Bashir Ahmad Malik^a, Mohd Washid Khan^a

^a Department of PG Studies and Research in Chemistry and Pharmacy, RD University, Jabalpur, MP, India

^b Department of Chemistry, Islamic University of Science and Technology, Awantipora, India

ARTICLE INFO

Keywords:

Sugar
Zn(II)
Synthesis
DFT
SOD
Antimicrobial
Anti-covid

ABSTRACT

In association with other antiviral drugs, Zinc is specially administered to the patients suffering from novel coronavirus infectious disease (nCOVID). Zn, maltol, and glucosamine are famous food and drug additives. The supplements made from them are helpful in minimizing malnutrition problems, and in enhancing immune power. Due to the well-pronounced effects of all these three components in the food and medicinal industry, a novel sugar Zn(II) complex of the general composition, $[Zn(gls)(mal)]$, where Hmal is maltol and Hgls is referred to as glucosamine, was synthesized and formulated. The physicochemical methods that were used to establish the molecular structure include elemental analysis, ¹HNMR, FT-IR, UV-Vis., thermal and mass spectrometry. Physical properties like decomposition temperature and molar conductance were also examined. The experimental results at each step of characterization were validated/compared with density functionalized spectroscopic/spectrometric data using the LANL2DZ basis set for the metal atom and 6–31 g(d,p) for other atoms under the B3LYP functional. From the study, a suitable square planar geometry is suggested for the complex. Among biological implications, superoxide dismutation (SOD) and antimicrobial actions were studied. Also, virtual screening using SWISS ADME and Autodock 4.0 program (against 6X2B, SARS-CoV-2 u1S2q 2 RBD Up Spike Protein Trimer) were evaluated for the complex. Good interactions were scored by glucosamine and the complex. The results obtained from antimicrobial sensitivity indicate low inhibition zones, but from the SOD data, the complex has shown satisfactory antioxidant behavior. Therefore, the proposed food supplement could act as a good antioxidant agent and could keep the flora of the intestinal tract less disturbed while going through a metabolic pathway.

1. Introduction

Zinc is an “essential trace element” mainly used for the prevention of zinc deficiency [1], and is also known as intelligence mineral [2]. Zinc plays important role in the maintenance of normal human growth and health, and therefore zinc supplements are used to prevent or treat zinc deficiency [3,4]. Lack of zinc may result in poor vision and delayed wound healing [5,6]. Therefore, the evaluation of zinc as a shield against human health abnormalities like the common cold, ear/respiratory infections, malaria, macular degeneration, cataracts, asthma, diabetes, high blood pressure, acquired immune deficiency syndrome (AIDS), acne, etc has gained fascination [7,8]. Even the possible treatment of dreadful disorders like Alzheimer’s disease,

Crohn’s disease, Hansen’s disease, Down syndrome, and anorexia nervosa has been linked with this element [9,10]. Natural dietary Zn-sources include chicken, red meat, and cereals [11]. The recommended amount of daily intake of zinc lies in the range of 5.21–12.48 mg/day [12].

Glucosamine on the other hand possesses multifunctional therapeutic potential and is found naturally in the human body [13]. But with aging, a considerable decrease in the levels of this compound begins, slowly leading to the bone-joint breakage [14]. Like zinc, glucosamine is also available in the market in suitable supplement forms. Generally, glucosamine is found in two main types of salts *viz* hydrochloride and sulphate [15]. This compound helps to keep cartilage healthy [16]. Some experts believe that glucosamine sulphate may help counteract

* Corresponding author. Department of PG Studies and Research in Chemistry and Pharmacy, RD University, Jabalpur, MP, India.

E-mail address: mirjanmohammad@gmail.com (J.M. Mir).

<https://doi.org/10.1016/j.jics.2022.100743>

Received 1 July 2022; Received in revised form 14 September 2022; Accepted 18 September 2022

Available online 29 September 2022

0019-4522/© 2022 Indian Chemical Society. Published by Elsevier B.V. All rights reserved.

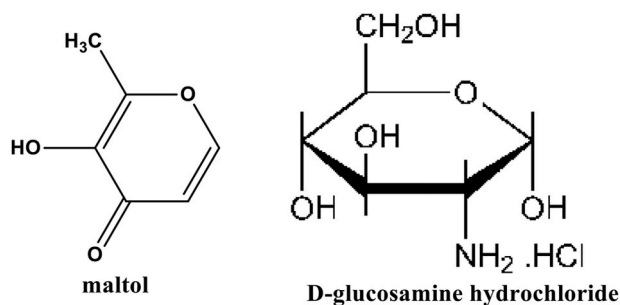


Fig. 1. 2-D structure of the ligands used in zinc(II) complexation.

this bone-joint effect [17]. Scientists have also proven that glucosamine can be used to treat rheumatoid arthritis, lung contamination, allergic infections, wounds, temporomandibular joint problems (TMJ), and back pain [18].

Maltol is also a natural organic compound commonly used as a flavor enhancer [19]. This compound is either extracted from plants like larch trees, pine needles, malt, and oils or maybe obtained synthetically [20]. This is a well-known “artificial sweetener” and good flavoring agent to produce a ‘fresh-baked’ taste and smell in bread, chocolate, soft drinks, ice cream, jam, etc. Cow’s milk is also used as a source of maltol [21]. It can be used in place of lactose by lactose-intolerant people. The suggested acceptable daily intake (ADI) of maltol is 2 mg/kg body weight [22]. Hence, maltol is an ideal food additive considered safe and non-toxic [23]. The compound bears remarkable anti-bacterial and anticorrosive properties. Due to corrosion inhibition, the compound can also serve as a food preservative [24].

Due to the conspicuous food and bio-medicinal properties of zinc(II), maltol and glucosamine, it is thus worthy to synthesize a complex of a collective and enhanced potentiality of its form containing all these three food additives (supplements). Therefore, this work describes the formulation and characterization of this compound involving physico-chemical techniques for this purpose. The respective experimental results have been validated with theoretical data. Density functional theory (DFT) based calculations with LANL2DZ/631-g(d,p) as basis set and B3LYP as functional have been employed in this study to elucidate theoretical spectroscopy, electron density plots, and other global reactive descriptors of the complex. Several experiments were laid to grow the single x-ray crystal of the complex but failed. Also, theoretical (molecular docking and SWISS ADME) and *in vitro* bioactivities have been evaluated for the complex to find the food supplement relevance of the compound. The ligands used in the work have shown in given in Fig. 1.

2. Experimental

2.1. Materials and methods

Zinc(II) sulphate heptahydrate was supplied by E. Merck India Chemicals, Bombay. D-Glucosamine hydrochloride and maltol were the products of Lancaster, UK, and Bengal Chemical and Pharmaceuticals Ltd., Kolkata, respectively. All the chemicals were used without any further purification. All the chemicals were of analytical reagent (A.R.) grade.

The elemental analysis was recorded on an Elemental Vario ELIII Carlo Erba 1108 analyzer. The content of zinc present in the complex was determined by EDTA-complexometric titration by following the similar procedure reported elsewhere [25]. Using the KBr pellet form of the complex, FT-IR spectral analysis of the complex was recorded on a Bruker α -T FTIR instrument. UV-Visible-NIR Spectrophotometer (Cary-5000), Agilent Technology Germany was employed to carry out the respective electronic spectral study. Mass spectral and ^1H NMR analyses were facilitated by SAIF-CDRI, Lucknow.

DFT based Theoretical calculation of the complex was carried out in a step-wise pattern. First of all, the molecular structure was optimized at the Becke3–Lee–Yang–Parr (B3LYP) hybrid exchange-correlation functional using standard 6–31 g(d,p)/LANL2DZ employing Gaussian09 program package [26,27]. After reaching the energy minimal geometry of the title complex (showing no imaginary frequency), theoretical spectral calculations, frontier orbital analysis, and other electron density plot computations were run using the respective commands accessible through the Gaussian09 associated animation program called as GaussView 5, that also serves as a visualization tool for various vibrational modes and other electron density maps [28]. Also, for virtual bioactivity screening SWISS ADME (online version) and Autodock 4.0 program were used.

2.2. Bioactivity tests

2.2.1. Superoxide dismutase activity

In vitro Superoxide dismutase activity was measured using alkaline DMSO as a source of superoxide radical ion O_2^- and nitrobluetetrazolium (NBT) as O_2^- scavenger. A fixed volume of 400 μL of the sample to be assayed was added to a solution containing 2.1 mL of 0.2 M potassium phosphate buffer (2.72 g in 100 mL distilled water) (pH 7.8) and 1 mL of 56 μM NBT in a test-tube. The tubes were kept in ice for 20 m and then 1.5 mL of alkaline DMSO solution (20 mg NaOH in 1 ml Water and 99 mL DMSO) was added while stirring. The absorbance was then monitored at 560 nm against a sample prepared under similar condition except that NaOH was absent in DMSO. The measurement of SOD activity, expressed as IC_{50} is the concentration of the substrate or complex, which causes 50% inhibition of the reduction of NBT [29].

2.2.2. Antibacterial sensitivity

The biological activity of the ligands and the complex was tested for their *in vitro* action against *Escherichia coli* by the agar well diffusion method using ampicillin as the standard drug. The selected bacteria were incubated into the beef-extract broth for 24 h. In this method, nutrient agar for bacteria and beef-extract agar sterilized in a flask and cooled to 50 $^\circ\text{C}$ was distributed (50 mL) to sterilized Petri dishes (10 cm in diameter) after injecting 0.1 mL cultures of the bacterium, prepared as mentioned above and allowed to solidify. By using a sterilized proper tube (5 mm diameter), wells were dug in the culture plates. The samples dissolved in dimethylformamide (DMF) with the concentrations of 100 ppm, 500 ppm, and 1000 ppm were added to these wells. The Petri dishes were left at 4 $^\circ\text{C}$ for 2 h and then the plates were incubated at 30 $^\circ\text{C}$ for bacteria for a period of 18–24 h. At the end of the period, inhibition zones formed on the medium were evaluated as millimeters (mm) diameter. DMSO served as the control during the study. The results were compared with a similar run of standard ampicillin (as an antibacterial). The antibacterial tests were calculated as a mean of three replicates [30,31].

2.3. Synthesis of the complex

The complex was prepared by following the slightly modified procedure reported elsewhere [25]. A solution of glucosamine hydrochloride (0.01 M, 2.15 g) in 20 mL methanol-water (50%) was neutralized with a 10 mL aqueous solution of sodium bicarbonate (0.01 M, 0.84 g). Afterward, the mixture was filtered. In another beaker 20 mL methanolic solution of 0.01 M (1.26 g) maltol was prepared. Both the mixtures were slowly added to a warm solution of $\text{ZnSO}_4 \cdot 7\text{H}_2\text{O}$ (0.01 M, 2.87 g), in ethanol (50%, 15 mL). The resulting ternary solution was allowed to reflux under constant stirring for 4 h until the desired complex was found to precipitate out, followed by suction filtration and washed several times with 1:1 ethanol-water solution, and dried *in vacuo*.

The overall schematic presentation of the synthesis is given below:

Analytical data: Chemical Formula: $\text{C}_{12}\text{H}_{17}\text{NO}_8\text{Zn}$, Molecular

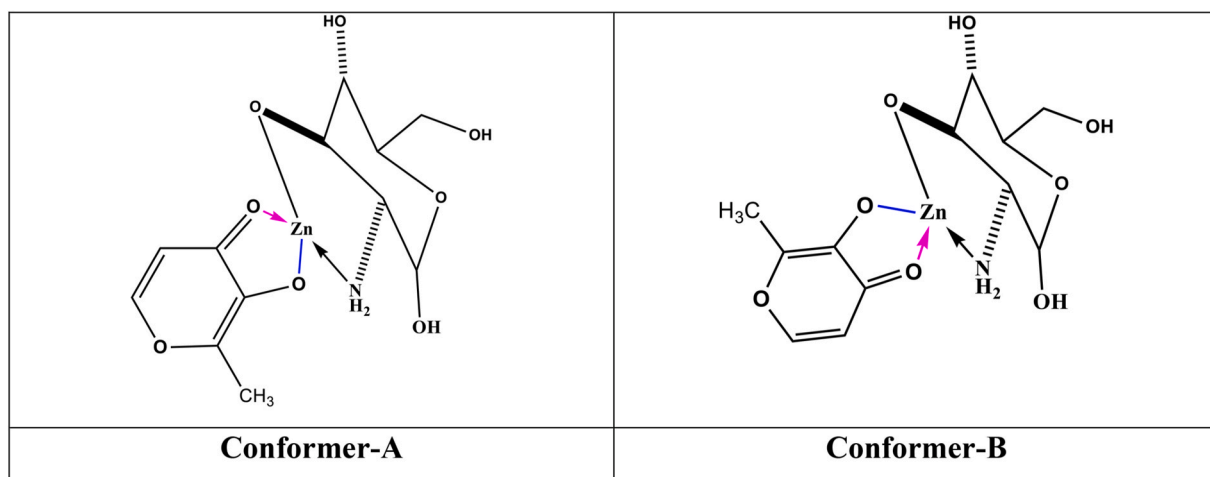


Fig. 2. 2D-Structure of the synthesized Zn(II) complex.

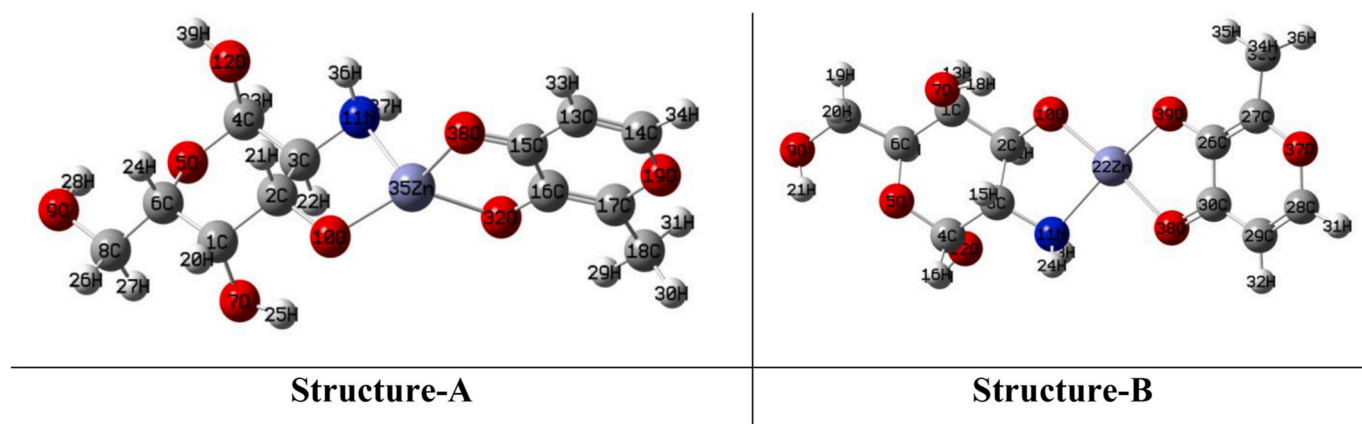


Fig. 3. Optimized structure of the complex in the two isomeric forms.

Weight: 368.65; m/z : 367, 369, 371, 149; Elemental Analysis (%): Found (theoretical): C, 39.07 (39.10); H, 4.63(4.65); N, 3.81(3.80); O, 34.70 (34.72); Zn, 17.70(17.74); FT-IR data (cm^{-1}): 540 (Zn–O), 810 (Zn–N), O–H (3419–3050), N–H (3419–3050), C–H (2939–2800), C=O_{maltol} (1624), C=C (1540–1566), C–O (1114–1276); UV–Vis data: 350–368 nm.

3. Results and discussion

The synthesized mixed ligand complex is air-stable white colored solid. The compound was found to show 230 °C as decomposition temperature. Solubility tests in various solvents showed that the complex is soluble in DMF, DMSO, and acetonitrile. The molar conductance determined for 1 mM, DMF solution of the complex indicates non-electrolytic behavior. To ascertain the proposed molecular

composition DFT-supported elemental analysis and other spectroscopic/spectrometric characterizations have been discussed and compared.

3.1. Geometry optimization

The suggested 2D-structure of the synthesized complex may be represented as given in Fig. 2 with the possible formation of two conformers.

Both the proposed isomers (conformer A and B) given in Fig. 2 were first of all optimized followed by frequency calculations to establish the most stable isoforms. In conformer-A, the enolic oxygen of maltol and –NH₂ groupings are in *cis* fashion in the coordination sphere, while as, in conformer B, both the functionalities are *trans* to one another. The level of theory applied for the respective calculations has furnished the structures given in Fig. 3 as the true minima of their potential surfaces

Table 1

Optimized parameters of the complex in the two isomeric forms.

Conformer-A		Conformer-B	
Connectivity	Bond Length (Å)	Connectivity	Bond Angle (°)
O(32)–Zn(35)	1.99	O(10)–Zn(35)–N(11)	86.73
O(10)–Zn(35)	1.92	O(10)–Zn(35)–O(38)	132.19
N(11)–Zn(35)	2.19	O(10)–Zn(35)–O(38)	129.72
O(38)–Zn(35)	2.07	N(11)–Zn(35)–O(32)	116.18
		N(11)–Zn(35)–O(38)	110.72
		O(32)–Zn(35)–O(38)	82.96
		Zn(22)–N(11)	2.20
		Zn(22)–O(38)	2.13
		Zn(22)–O(39)	2.04
		Zn(22)–O(10)	1.98
		O(38)–Zn(22)–O(10)	174.10
		N(11)–Zn(22)–O(39)	166.29
		N(11)–Zn(22)–O(38)	90.33
		O(38)–Zn(22)–O(39)	80.26
		O(38)–Zn(22)–O(10)	103.71
		N(11)–Zn(22)–O(10)	84.99

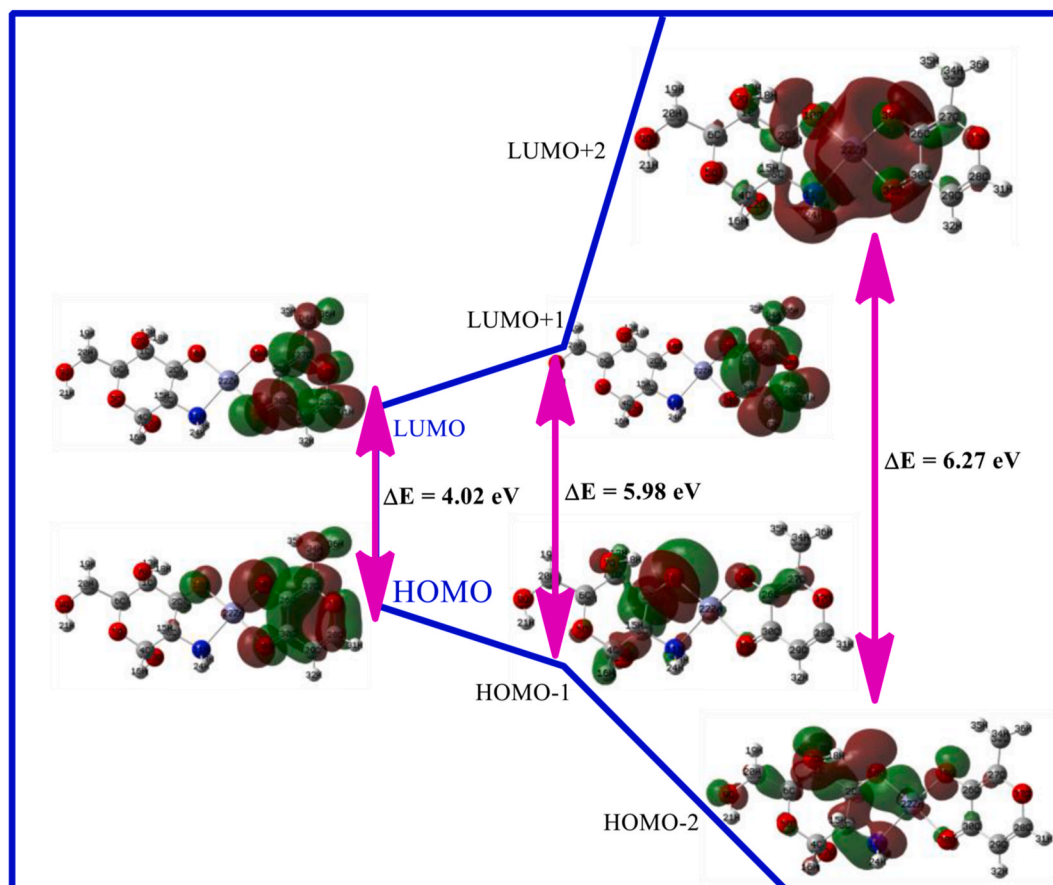


Fig. 4. FMO-diagram of the complex with the respective energy gaps.

showing no imaginary frequency. The geometric parameters of the complex under question *viz* bond lengths and bond angles for both the computed isoforms have been given in Table 1. From the tabulated data it is confirmed that the complex in structure form-A bears distorted square planar (irregular tetrahedral) geometry, and while a suitable square planar geometry is found in the case of isomer-B. The distortion in the former may be because of enantiomeric shift generally seen in glucosamine moiety, and the $>C=O-Zn$ of maltol part is found out of the plane in comparison with the other three coordination bindings within the sphere. The same explanation can be made in terms of bond lengths stemming from the magnitude of distortion in square planarity. However, in the structure-B, suitable square planarity in terms of bond lengths and bond angles is quite evident. In order to decide which of the two conformations represents more stable isomer, suitable zero-point energy (ZPE) calculation was done, indicating the ZPE value of 794003 J/mol in former and 792064 J/mol in latter. Also, the molecular orbital calculations for both the structural frameworks show a 3.26 eV HOMO-LUMO gap for A, whereas, in B it is 4.02 eV. Therefore, the stability is well pronounced in the B-form of the complex. Hence, all the theoretical data confined to the square planar geometry of the complex has been comparatively discussed with the respective characterization related to the formulation. The results are comparable with the similar complexes reported elsewhere [32,33].

In order to verify the formation constant or stability constant, spectrophotometric method using the modified procedure of Hilderbrand and Benesi as described by Rose and Drago [34] was used. A series of solutions were prepared with a constant concentration of metal ion [M] and variable ligand, [L] concentration. The absorbance of each of the mixtures was taken at λ_{max} previously determined and the stability constant, β was determined using equation. $M/A = 1/\beta\epsilon_c[1/L_0] + 1/\epsilon_c$. Plot of M/A versus 1/L gives the intercept $1/\epsilon_c$ and slope $1/\beta\epsilon_c$ from

which β (stability constant) can be evaluated. The same verification was done using potentiometric method. From both the methods Stability constant comes out to be 4.10, in relevance with the suggested geometry [32,33].

3.2. Frontier molecular orbital (FMO) analysis

In addition to geometry elucidation frontier orbital analysis also supports the projection of both HOMO and LUMO electron density along the maltol side of the complex (Fig. 4). 4.02 eV is the energy band gap (ΔE) between HOMO and LUMO. The HOMO-1, HOMO-2, LUMO+1, and LUMO+2, with their corresponding energy gaps, have also been given. The ionization energy (IE) and electron affinity (EA) in relation to frontier orbitals reveal the respective values as 0.22 and 0.07 a.u., respectively [35]. The other two global reactive descriptors including absolute electronegativity (χ_{abs}) and absolute hardness (η) may further, be evaluated by taking $1/2(IE + EA)$ meant for χ_{abs} and η maybe evaluated as $1/2(IE-EA)$ [36].

3.3. Spectroscopic and spectrometric analysis

The experimentally recorder FT-IR spectrum of the synthesized complex along with the corresponding theoretically generated spectrum obtained at DFT/B3LYP level of theory using 6-311G/LANL2DZ basis sets is represented by Fig. 5.

The important vibrational modes of the complex in and around the coordination sphere are important in discussing the metal-ligand binding fashion. The three functional identities of Zn-O and single Zn-N confined to the coordination zone lie in the range of 540–810 cm^{-1} indicating the metal anchoring identification of hydroxyl groups and amine nitrogen. This region is very significant in establishing the

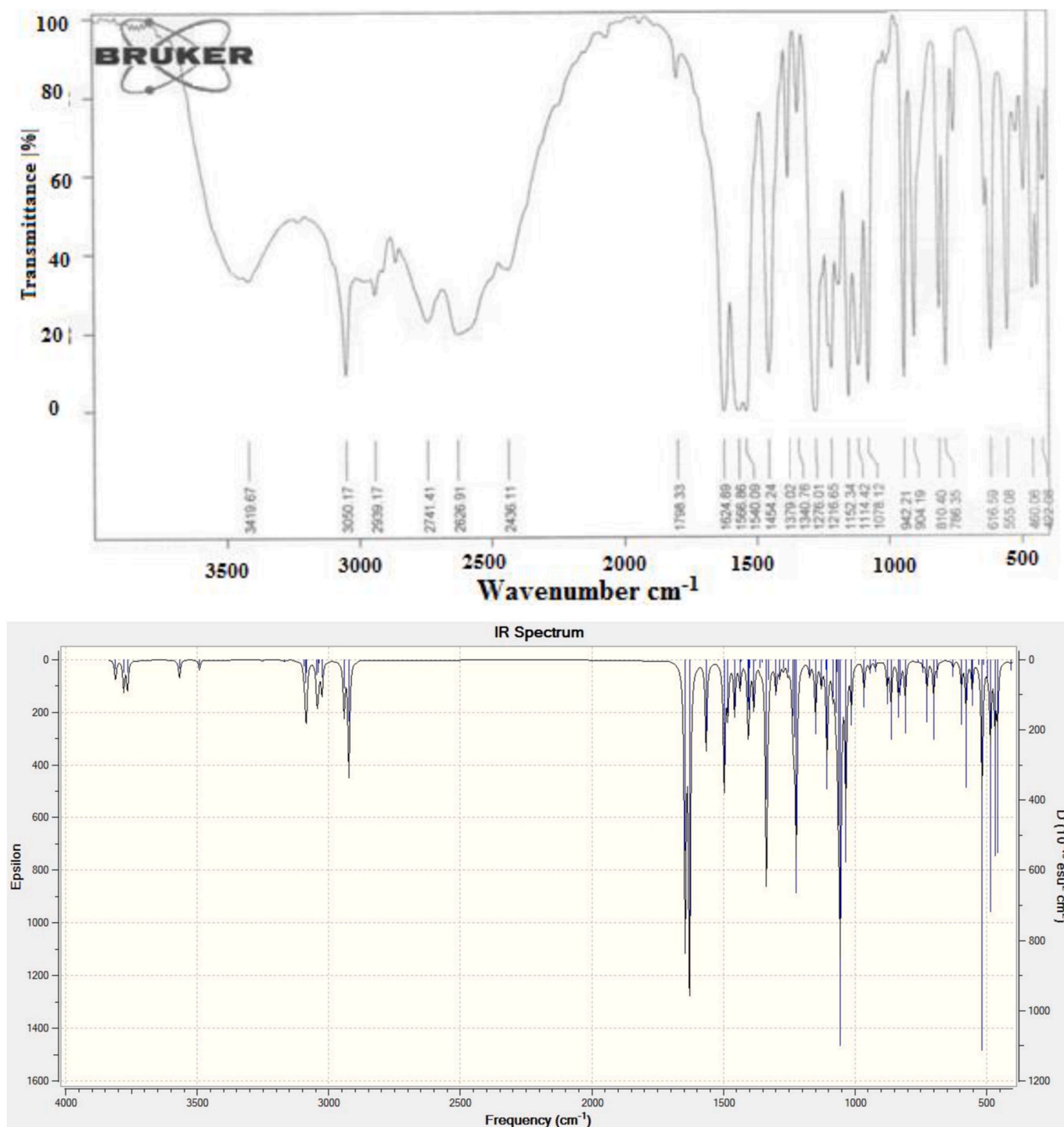
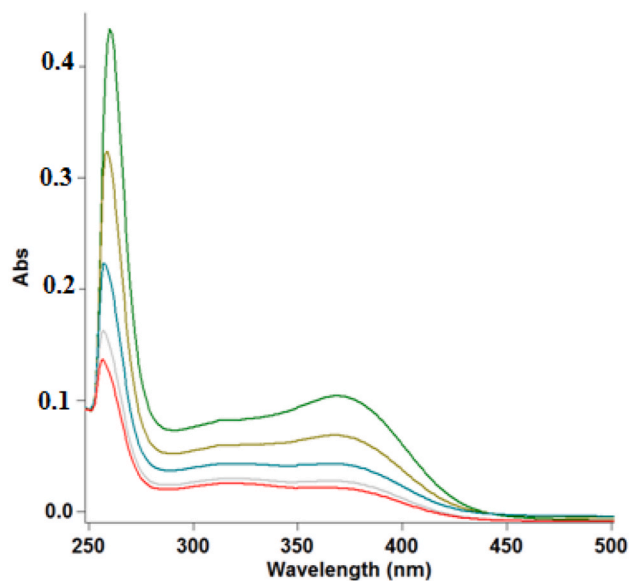


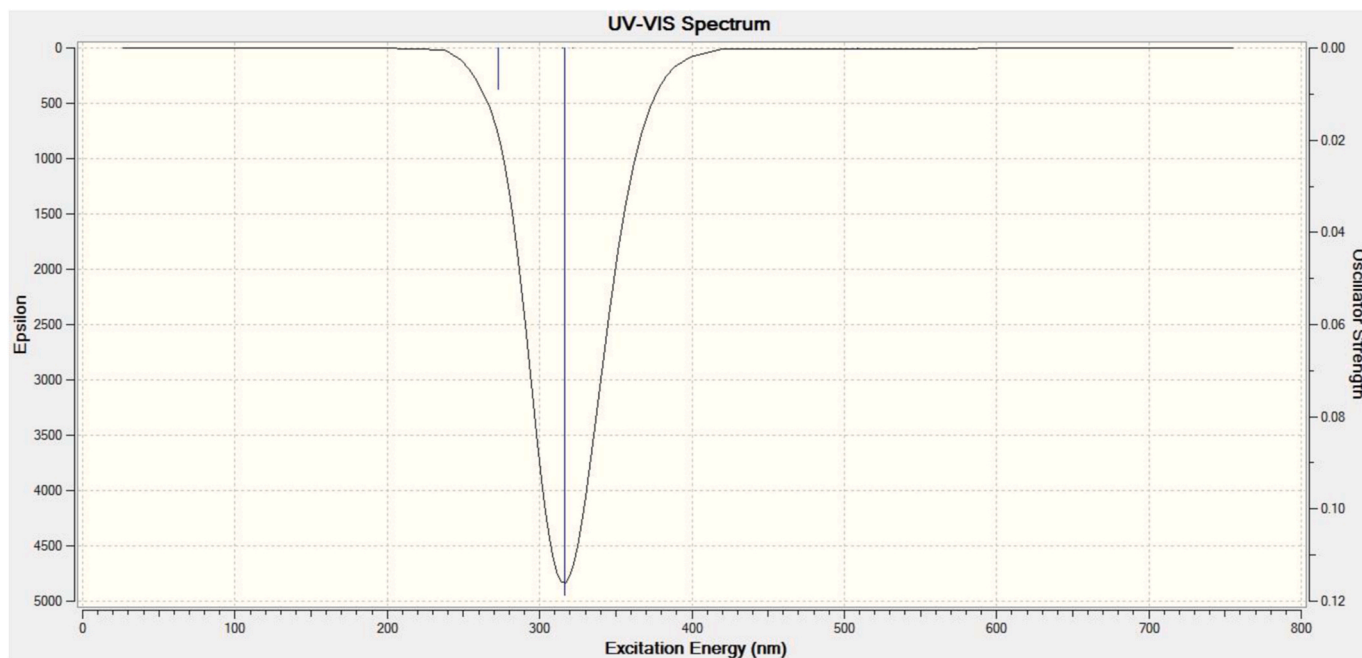
Fig. 5. Experimental (a) and Theoretical, (b) FT-IR spectra of the complex.

certainty of the metal complex. Comparing theoretical data with experimental results assures the close reliability of the theory applied in the calculation. Considering the glucosamine moiety of the complex, the fundamental vibrations of this part include O–H and N–H stretching band in the range $3419\text{--}3050\text{ cm}^{-1}$ and C–H stretching band in $2939\text{--}2800\text{ cm}^{-1}$. Maltol exhibits a fundamental vibrational frequency of carbonyl group at 1624 cm^{-1} which is different from the normal carbonyl group absorption depicting the coordination of this atom with metal. The range of $1540\text{--}1566\text{ cm}^{-1}$ is because of C=C vibrations. The different C–O absorptions are assignable at $1114\text{--}1276\text{ cm}^{-1}$. This again certifies the binding mode of enolic part of both the title ligands [37].

To explain the binding pattern of the complex one is primarily interested to find the electronic spectral elucidation of a compound. The UV–Visible spectrum of the complex was recorded in three different serially diluted DMSO solutions (1, 2, and 3 mM) and the results indicate the existence of two intra-ligand transitions in the ultraviolet region ($270\text{--}370\text{ nm}$). The respective experimental spectrum has been comparatively presented in Fig. 6. From the experimental observations, it was observed that the nature of absorbance was similar throughout the different concentrations. However, the increase in concentration has shown an increase in absorbance. These electronic transitions are indicative of the square planar geometry of the complex consistent with



(b)



(a)

Fig. 6. Experimental (a) and Theoretical (b) UV-Vis. spectra of the complex.

Table 2

TD-DFT electronic excitation data of the complex.

Orbital assignment	λ_{max} (nm)	Energy of Excitation (eV)	Oscillator Strength (<i>f</i>)	Excitation probability (%)
HOMO→LUMO+1	273	4.54	0.0090	63
HOMO→LUMO+2	273	4.54	0.0090	33
HOMO→LUMO	316	3.92	0.1187	95

the data reported elsewhere [38–41].

Time dependant-density functional theory (TD-DFT) based energy calculation of the complex revealed that the experimentally observed results are comparable to the theoretical outcomes. The non-zero oscillator strength confirms acceptability of transition energies within the nature of excitation among different sets of FMOs [18]. The related computed data have been presented in Table 2. Theoretically generated spectrum supports the experimental UV-Visible results by displaying only two absorptive peaks almost in the similar range having the feature of intra-ligand transitions [42].

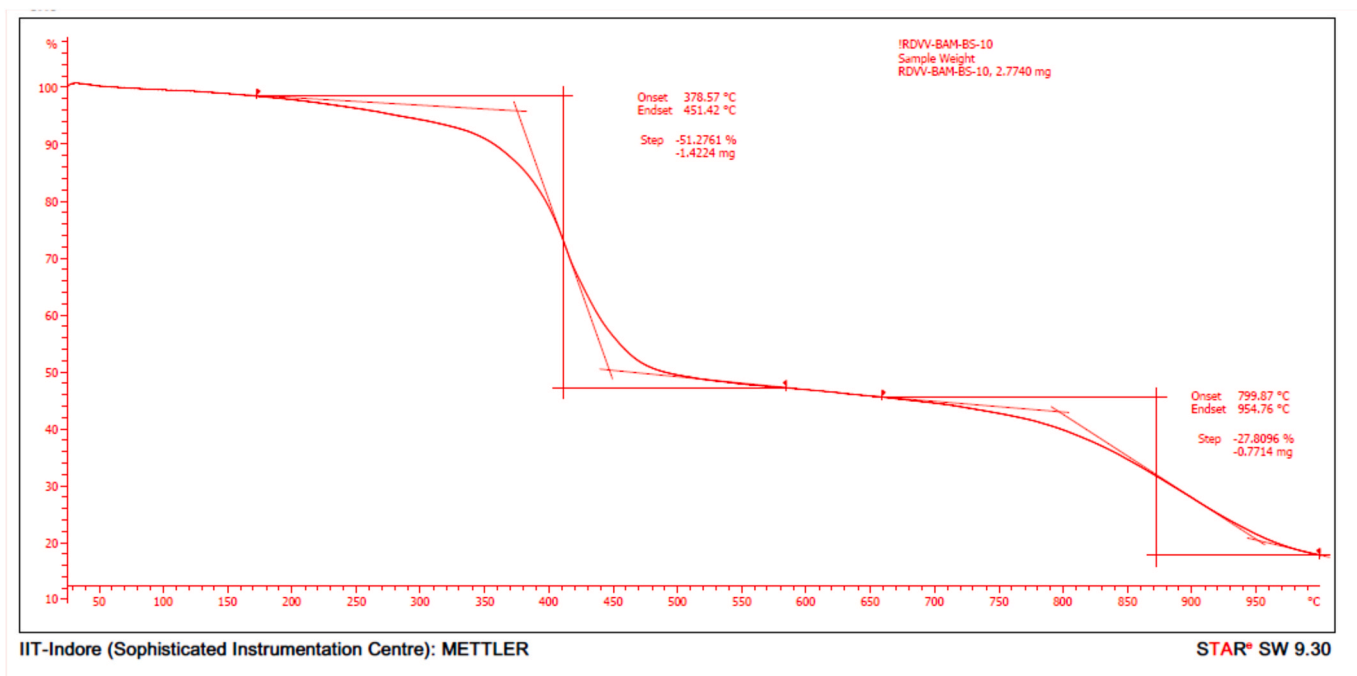


Fig. 7. TG-curve of the representative complex.

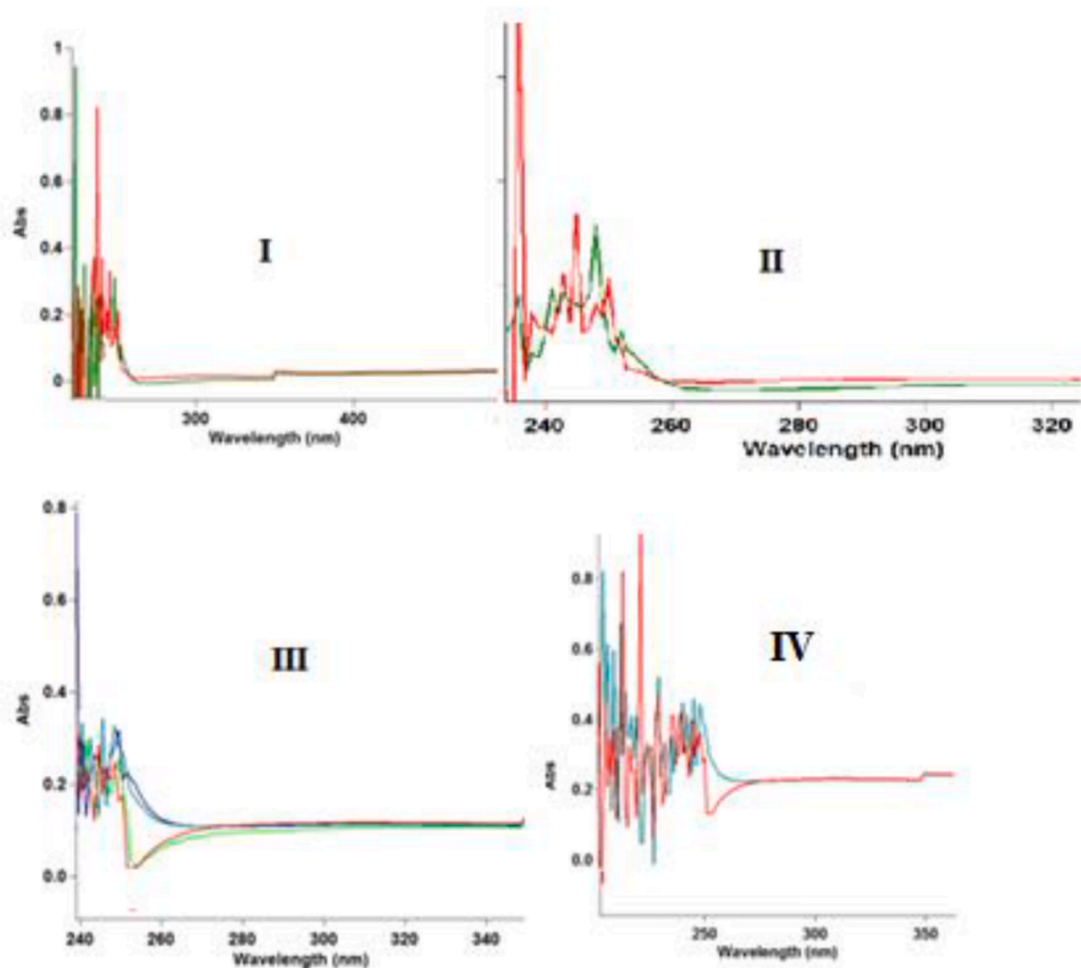


Fig. 8. UV-Visible spectra (at several μM concentrations) recorded for (I) Zinc sulphate, (II) Zinc complex, (III) Maltol and (IV) glucosamine.

3.4. Thermal behaviour

The thermal behavior of the representative zinc complex (Fig. 7) was carried out at IIT-Indore using METTLER instrument in the temperature range 27–1050 °C at a heating rate (°C/min) of 10. The compound was found to show the decomposition in two steps that finally form the zinc oxide. The compound in its first decomposition step shows a weight loss of 51.28% (near 170–600 °C) referring to the removal of glucosamine moiety plus ring methyl group of maltol. This is in close approximation with the calculated value of 52.71% for the initial step. The second step involves the mass elimination of maltol minus methyl group (already lost in the first step) and an oxygen atom (O remaining attached with Zn) which is noticeable at 650–900 °C, (obsd. = 27.80%, calcd. = 25.81%). The final weight residue (ZnO) which is the most stable state during the thermal degradation process is clearly detected at 950 °C with the observed mass percentage of 21% (Calcd. 22.01%). The overall pyrolytic insights stem from the assumptions made for the structural verification in the FT-IR and electronic spectral data (*vide supra*) and may further be clarified by elemental analysis and mass spectral data. From both the analysis the composition of the complex gets ascertained [43,44].

The ESI-mass spectrum (Fig. S1) clearly indicates the m/z 367, 369, and 371 for the molecular mass of the complex and isotopic effect of zinc. The 149 is also factual of supporting molecular ion in di-positive mode. Fig. S2 is the ¹H NMR spectrum of the complex recorded in DMSO as a solvent. The respective proton assignments have been given in the figure and give clear support for the suggested composition of the complex. The calculated spectrum supports the experimentally observed resonating signals.

4. Biological implications

4.1. Evaluation of SOD mimic properties

The complex under question bears significant superoxide dismutase activity. By virtue of this property, the complex can be used as a defense in scavenging biologically produced free radical species. The metallic ion oxidation state, geometry, and nature of ligation play important role in designing intelligent Superoxide dismutase (SOD)-mimic complexes. In the present study, Nitro blue tetrazolium chloride (NBT) assay was followed by the recording of the absorbance that renders kinetic reduction of NBT at 560 nm. The IC₅₀ values evaluated under the given assay for the ligand Hgls and the mixed ligand complex were found to be 31 and 38 μM, respectively.

It is a known fact that Cu–Zn association is mainly the duet metal component that expresses super oxide activity in biological processes. In case of the investigated metallic complex, in order to find the SOD-responsible moiety of the compound the glucosamine, maltol, zinc sulphate and the complex itself were tested separately for the SOD-activity and the respective absorption spectra have been given in Fig. 8. From the calculated values and the behavior of the species it looks glucosamine and maltol as the main part responsible for the SOD-action. Glucosamine and maltol show 31 and 35 μM activity and hence the role of Zn is only to act as a carrier of two SOD-active ligands. The ketonic and hydroxyl functionalities could be thus supportive of proton transfer under the respective reaction. Hence, redox pathways whether forward or backward both are the real tendencies to show SOD-mimic potential [40,41].

4.2. Antibacterial study

In the present investigation, both the ligands are of pharmacological importance coupled with Zinc. The biological activity was tested against *Escherichia coli* which is an anaerobic gram-negative bacterium belonging to the family *Enterobacteriaceae*. This microbe occurs in the lower portion of the intestine of human and warm-blooded animals, where it is a part of normal flora. *Escherichia coli* is an opportunistic pathogenic bacteria, causing disease mainly to the people having weak

Table 3
Antibacterial data of the compounds.

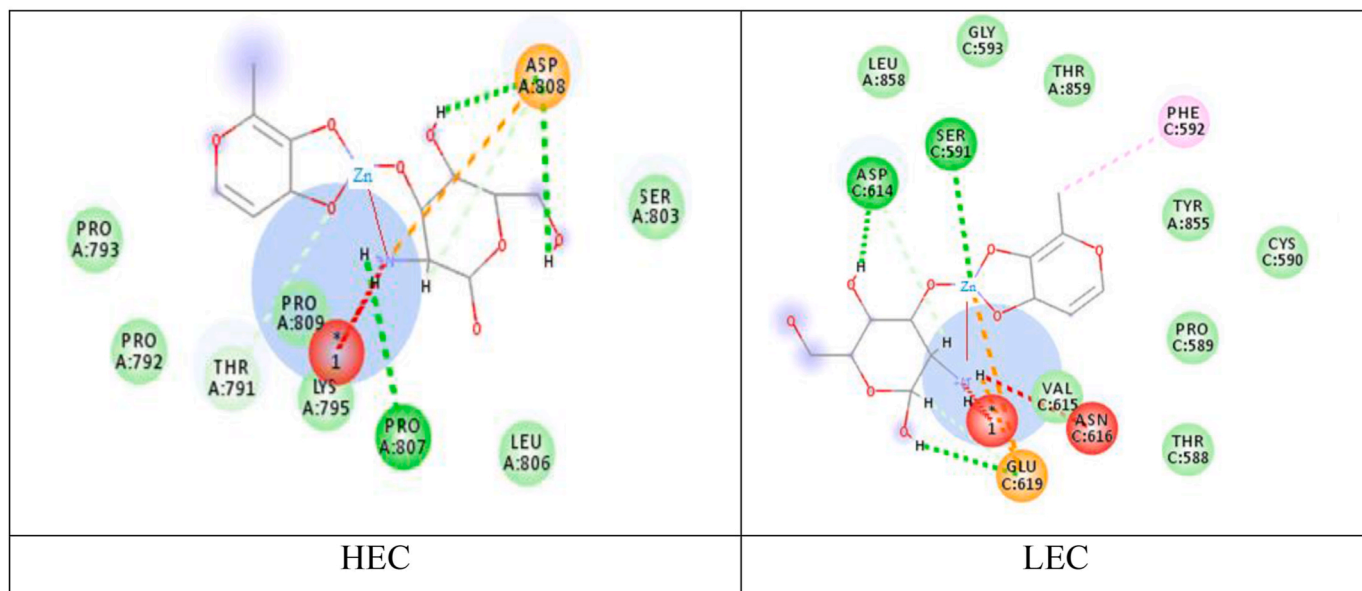
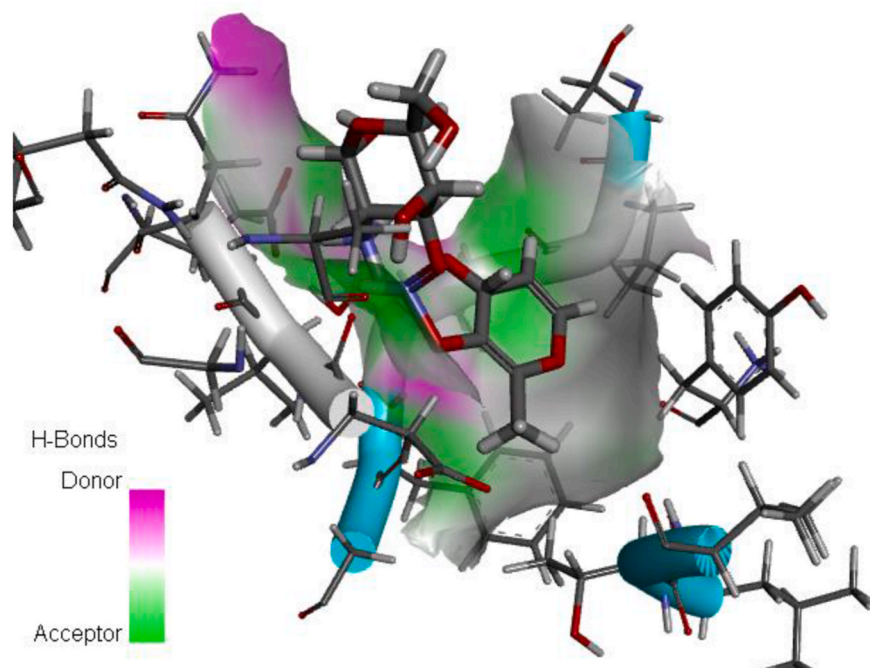
Concentration (ppm)	Compounds			
	Hmal	Hgls	complex	Ampicillin
	←————— Inhibition zones(mm) —————→			
100	20	10	20	32
200	22	12	30	38
300	20	13	32	45
DMSO	0	0	0	0

immune system. The antibacterial actions of the ligands, Hgls and Hmal and the respective metal complex indicate enhanced activity shown by the complex. The result of the antibacterial screening of the ligands and complex are compared in Table 3. From the IC₅₀ values 482 for Hmal, 883 for Hgls, and 378 for the complex, it is obvious that the complex is not as strong bactericidal as ampicillin, but is more active as compared to the respective ligands. Moreover, among food properties, it is advisable that the food supplement should not destroy the flora of the intestine, and hence, the results obtained in the investigation indicate an E. coli-friendly Zn-complex.

4.3. Anti-covid virtual screening

In the prevailing apocalyptic covid times, efforts are in process to develop a successful vaccine against this dreadful disease. Many virtual screening tests are reported every day to represent successful anti-covid drugs. To test glucosamine and its complex for the same, Autodock 4.0 was employed to find the fitting score against 6X2B PDB code representing coronavirus (CoV) spike (S) protein, involved in viral–host cell fusion. From the results given for the complex, a total of 100 conformations were generated with the score of Highest Energy Conformation (Zn_HEC) was (–2.22) and the score of Lowest Energy Conformer (Zn_LEC) was found to be (–5.12). The interactions are given in Fig. S3 (meant for Hgls showing –3.5 to –2.23 as LEC and HEC, respectively) are virtually low as compared to the complex docking score shown in Fig. 9. The non-bonding interaction plays an important part in the respective interaction. The anticoronavirus drug designing involves two main mechanistic approaches *viz*, a fusion of biomembrane through interaction with the receptors of viral surface, and secondly to halt the RNA-replication. In the present case, the several structural interactions of the complex show efficient hydrogen bonding with the spike protein. Both the LEC and HEC interactions have been given in the respective color code. With this aim, we performed an *in silico* comparative modeling analysis, which allows gaining new insights into the main conformational changes occurring in the SARS-CoV-2 spike protein, at the level of the receptor-binding domain (RBD), along interactions with human cells angiotensin-converting enzyme 2 (ACE2) receptor, that favor human cell invasion.

In Fig. 10 the color mapping of this complex generated via DFT calculations shows a promising three region locations based on charge density [45]. This molecular topology representation is generally called a molecular electrostatic potential surface (MESP), wherein the molecular reactivity of a molecule is explained on the basis of the charge of different regions [46,47]. These negative, positive, and neutral locations represented by color-coding. The MESP in the present case shows carbonyl oxygen as the most negative part, while hydroxyl/enolic oxygen is the region of moderate negative potential. The amine part has been shown as the electropositive section near the coordination sphere. Comparing these results with the docking poses shows excellent agreement in finding the role of non-covalent or electrostatic interaction in inhibiting SARS-CoV spike protein.



Interactions

- van der Waals
- Salt Bridge
- Conventional Hydrogen Bond
- Unfavorable Negative-Negative
- Unfavorable Donor-Donor
- Pi-Alkyl
- Carbon Hydrogen Bond

Fig. 9. Docking interaction of the complex.

4.4. ADME analysis

ADME refers to an important abbreviated form of “absorption, distribution, metabolism, and excretion” usually studied in

pharmacokinetics and pharmacology. Generally, online servers like <http://www.swissadme.ch/>, <https://www.molinspiration.com/> etc are referred for this computation. The description of the disposition of a compound within an organism can be made by using ADME analysis.

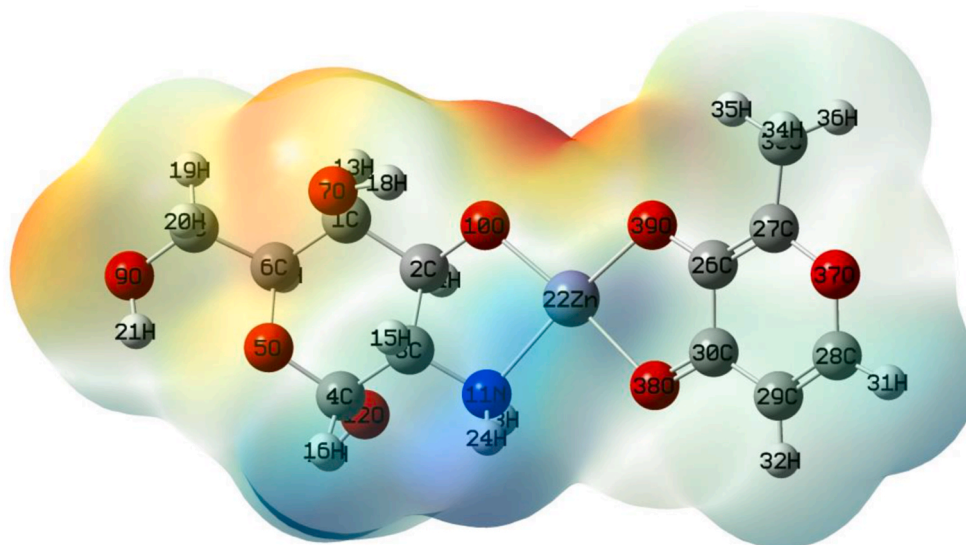


Fig. 10. MESP of the complex.

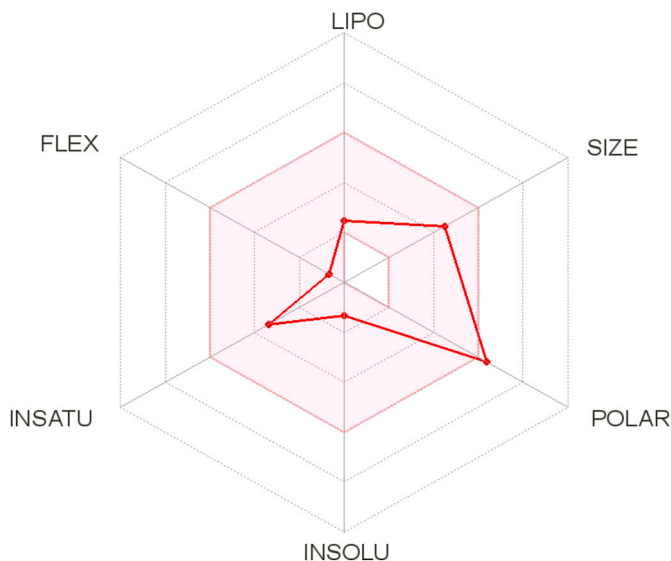


Fig. 11. Egg-shell model of ADME analysis of the complex.

The four criteria all influence the drug levels and kinetics of drug exposure to the tissues and hence influence the performance and pharmacological activity of the compound as a drug. Fig. 11 displays the parameters representing the fascinating properties of the complex under discussion. The solubility, lipophilicity and other drug likeness parameters indicate biomedical properties linked with the complex [48,49].

5. Conclusions

A square planar complex of zinc-containing maltol and glucosamine is revealed. The theoretical data significantly validates the assumptions made in experimental observations. The compound is a three in one food additive and may be further subjected to undergo feed trials to declare the molecule as a health supplement. Among food properties the SOD as an antioxidant (most beneficial for COVID-19 patients), intestinal flora friendly, and spike protein fusion properties all remark the finding to declare such a complex as a food supplement for covid-19 patients in particular and as a health supplement for general. Furthermore, our analysis provides an ideal pipeline to identify the set-up of the right

biological molecular context for investigating spike RBD-ACE2 interactions for the development of new vaccines, diagnostic kits, and other treatments based on the targeting of SARS-CoV-2 spike protein. More biological investigations shall reveal its more food-like signatures.

Declaration of competing interest

The authors declare that they have no known competing financial interests or personal relationships that could have appeared to influence the work reported in this paper.

Acknowledgement

Authors are thankful Sophisticated Analytical Instrument Facility, CDRI, Lucknow for Mass and CHN analysis. We also acknowledge the Department of Chemistry and Pharmacy, Rani Durgavati University, Jabalpur for providing Lab facilities and Instruments.

Appendix A. Supplementary data

Supplementary data to this article can be found online at <https://doi.org/10.1016/j.jics.2022.100743>.

References

- [1] P.T. Bhattacharya, S.R. Misra, M. Hussain, Nutritional aspects of essential trace elements in oral health and disease: an extensive review, *Sci. Tech. Rep.* (2016), <https://doi.org/10.1155/2016/5464373>, 2016.
- [2] A.R. Putri, A. Anwar, E. Chasanah, Y.N. Fawzya, P. Martosuyono, Nuryanto, D. N. Afifah, Analysis of iron, calcium and zinc contents in formulated fish protein hydrolyzate (FPH) complementary feeding instant powder, *Food Res.* 4 (Suppl. 3) (2020) 63–66, [https://doi.org/10.26656/fr.2017.4\(S3\).S09](https://doi.org/10.26656/fr.2017.4(S3).S09).
- [3] A. El-Bakry, A.M. El Safty, A.A. Abdou, O.R. Amin, D.R. Ayoub, D.Y. Afifi, Effect of zinc supplementation in zinc-deficient children with attention-deficit hyperactivity disorder, *Egypt. J. Psychiatr.* 40 (2019) 86–94.
- [4] A.A. El Taweel, R. Salem, A. Allam, Intraleisional 2% zinc sulfate solution for plane warts: a case report, *Dermatol. Ther.* 32 (1) (2019), e12761, <https://doi.org/10.1111/dth.12761>.
- [5] R.B. Saper, R. Rash, Zinc: an essential micronutrient, *Am. Fam. Physician* 79 (9) (2009) 768–772.
- [6] M. Dardenne, Zinc and immune function, *Eur. J. Clin. Nutr.* 56 (3) (2002) S20–S23.
- [7] G. Bjorklund, M. Dadar, L. Pivina, M.D. Doğa, Y. Semenova, J. Aaseth, The role of zinc and copper in insulin resistance and diabetes mellitus, *Curr. Med. Chem.* 27 (39) (2020) 6643–6657.
- [8] J. Olechnowicz, A. Tinkov, A. Skalny, J. Suliburska, Zinc status is associated with inflammation, oxidative stress, lipid, and glucose metabolism, *J. Physiol. Sci.* 68 (2018) 19–31.

- [9] N. Roohani, R. Hurrell, R. Kelishadi, R. Schulin, Zinc and its importance for human health: an integrative review, *J. Res. Med. Sci.* 18 (2) (2013) 144–157.
- [10] K. Kerns, M. Zigo, P. Sutovsky, Zinc: a necessary ion for mammalian sperm fertilization competency, *Int. J. Mol. Sci.* 19 (12) (2018) 4097, <https://doi.org/10.3390/ijms19124097>.
- [11] B.M. Bohrer, Nutrient density and nutritional value of meat products and non-meat foods high in protein, *Trends Food Sci. Technol.* 65 (2017) 103–112.
- [12] T. Filippini, S. Cilloni, M. Malavolti, F. Violi, C. Malagoli, M. Tesaro, I. Bottecchi, A. Ferrari, L. Vescovi, M. Vinceti, Dietary intake of cadmium, chromium, copper, manganese, selenium and zinc in a Northern Italy community, *J. Trace Elem. Med. Biol.* 50 (2018) 508–517.
- [13] R. Dalirfardouei, G. Karimi, K. Jamialahmadi, Molecular mechanisms and biomedical applications of glucosamine as a potential multifunctional therapeutic agent, *Life Sci.* 152 (2016) 21–29.
- [14] S. Lu, M.B. Haskali, K.M. Ruley, N.J. Dreyfus, S.L. DuBois, S. Paul, J.S. Liow, C. L. Morse, A. Kowalski, R.L. Gladding, J. Gilmore, PET ligands [18F] LSN3316612 and [11C] LSN3316612 quantify O-linked- β -N-acetyl-glucosamine hydrolase in the brain, *Sci. Transl. Med.* 12 (543) (2020), eaau2939, <https://doi.org/10.1126/scitranslmed.aau29>.
- [15] O.F. Restaino, R. Finamore, A. Stellavato, P. Diana, E. Bedini, M. Trifuoggi, M. De Rosa, C. Schiraldi, European chondroitin sulfate and glucosamine food supplements: a systematic quality and quantity assessment compared to pharmaceuticals, *Carbohydr. Polym.* 222 (2019), 114984, <https://doi.org/10.1016/j.carbpol.2019.114984>.
- [16] S. Tenti, N. Giordano, N. Mondanelli, S. Giannotti, E. Maheu, A. Fioravanti, A retrospective observational study of glucosamine sulfate in addition to conventional therapy in hand osteoarthritis patients compared to conventional treatment alone, *Aging Clin. Exp. Res.* 32 (2020) 1161–1172.
- [17] R.C. Maurya, B.A. Malik, J.M. Mir, A.K. Sharma, Synthesis, characterization, thermal behavior, and DFT aspects of some oxovanadium(IV) complexes involving ONO-donor sugar Schiff bases, *J. Coord. Chem.* 67 (18) (2014) 3084–3106.
- [18] J.M. Mir, D. Kumar Rajak, R. Charitra Maurya, Bio-conjugated N-(2-hydroxy-1-naphthaldehyde)-glucosamine Cu (II) complex: bacterial sensitivity and superoxide dismutase-like activity, *J. Coord. Chem.* 71 (14) (2018) 2225–2242.
- [19] L.F. Bjeldanes, H. Chew, Mutagenicity of 1, 2-dicarbonyl compounds: maltol, kojic acid, diacetyl and related substances, *Mutat. Res. Genet. Toxicol.* 67 (4) (1979) 367–371.
- [20] E. Macedi, D. Paderni, M. Formica, L. Conti, M. Fanelli, L. Giorgi, S. Amatori, G. Ambrosi, B. Valtancoli, V. Fusi, Playing with structural parameters: synthesis and characterization of two new maltol-based ligands with binding and antineoplastic properties, *Molecules* 25 (4) (2020) 943.
- [21] S. Patton, R.J. Flipse, Studies of heated milk. V. The reaction of lactose with milk protein as shown by lactose-1-C14, *J. Dairy Sci.* 36 (7) (1953) 766–771.
- [22] J. Peng, M. Wei, Y. Hu, Y. Yang, Y. Guo, F. Zhang, Simultaneous determination of maltol, ethyl maltol, vanillin, and ethyl vanillin in foods by isotope dilution headspace solid-phase microextraction coupled with gas chromatography-mass spectrometry, *Food Anal. Methods* 12 (8) (2019) 1725–1735.
- [23] A.H. Aktas, Spectrometric multi component determination of maltol, ethyl maltol, vanillin and ethyl vanillin in foods by multi linear regression calibration, classical least square and inverse least square methods, *Asian J. Chem.* 22 (5) (2010) 3719–3728.
- [24] J.M. Mir, R.C. Maurya, P.K. Vishwakarma, Corrosion resistance and thermal behavior of acetylacetonato-oxoperoxomolybdenum (VI) complex of maltol: experimental and DFT studies, *Karala Int. J. Mod. Sci.* 3 (4) (2017) 212–223.
- [25] J.M. Mir, R.C. Maurya, D.K. Rajak, B.A. Malik, P.S. Jaget, N. Jain, A novel Schiff base complex of brain fuel (sugar) coordinated with intelligence mineral (Zn): synthesis, conjoint DFT-experimental evaluation and super oxide dismutation, *Karala Int. J. Mod. Sci.* 3 (3) (2017) 153–164.
- [26] M.J. Frisch, W. Trucks, G. H.B. Schlegel, G.E. Scuseria, M.A. Robb, J.R. Cheeseman, G. Scalmani, V. Barone, B. Mennucci, G.A. Petersson, H. Nakatsuji, M. Caricato, X. Li, H.P. Hratchian, A.F. Izmaylov, J. Bloino, G. Zheng, J.L. Sonnenberg, M. Hada, M. Ehara, K. Toyota, R. Fukuda, J. Hasegawa, M. Ishida, T. Nakajima, Y. Honda, O. Kitao, H. Nakai, T. Vreven, J.A. Montgomery, J.E. Peralta, F. Ogliaro, M. Bearpark, J.J. Heyd, E. Brothers, K.N. Kudin, V.N. Staroverov, T. Keith, R. Kobayashi, J. Normand, K. Raghavachari, A. Rendell, J.C. Burant, S.S. Iyengar, T. Tomasi, M. Cossi, N. Rega, J.M. Millam, M. Klene, J.E. Knox, J.B. Cross, V. Bakken, C. Adamo, J. Jaramillo, R. Gomperts, R.E. Stratmann, O. Yazyev, A. J. Austin, R. Cammi, C. Pomelli, J.W. Ochterski, R.L. Martin, G. Morokuma, V. G. Zakrzewski, G.A. Voth, Salvador, P. J.J. Dannenberg, Dapprich, S. A.D. Daniels, O. Farkas, J.B. Foresman, J.V. Ortiz, Cioslowski, D.J. Fox, GAUSSIAN 09 (Revision C.01), Gaussian, Inc., Wallingford CT, 2010.
- [27] J.M. Mir, N. Jain, B.A. Malik, R. Chourasia, P.K. Vishwakarma, D.K. Rajak, R. C. Maurya, Urinary tract infection fighting potential of newly synthesized ruthenium carbonyl complex of N-dehydroacetic acid-N'-o-vanillin-ethylenediamine, *Inorg. Chim. Acta.* 467 (2017) 80–92.
- [28] J.M. Mir, R.C. Maurya, A new Ru (II) carbonyl complex of 2-benzoylpyridine: medicinal and material evaluation at the computational-experimental convergence, *J. Chinese Adv. Materials Soc.* 6 (2) (2018) 156–168.
- [29] P.K. Vishwakarma, J.M. Mir, R.C. Maurya, Pyrone-based Cu (II) complexes, their characterization, DFT based conformational drift from square planar to square pyramidal geometry and biological activities, *J. Chem. Soc. (Bangalore, India)* 128 (4) (2016) 511–522.
- [30] F.A. Hamill, S. Apio, N.K. Mubiru, R. Bukenya-Ziraba, M. Mosango, O.W. Maganyi, D.D. Soejarto, Traditional herbal drugs of Southern Uganda, II: literature analysis and antimicrobial assays, *J. Ethnopharmacol.* 84 (1) (2003) 57–78.
- [31] M.T. Baratta, H.D. Dorman, S.G. Deans, A.C. Figueiredo, J.G. Barroso, G. Ruberto, Antimicrobial and antioxidant properties of some commercial essential oils, *Flavour Fragrance J.* 13 (4) (1998) 235–244.
- [32] T. Dudev, C. Lim, Tetrahedral vs octahedral zinc complexes with ligands of biological interest: a DFT/CDM study, *J. Am. Chem. Soc.* 122 (45) (2000) 11146–11153.
- [33] R.R. Roe, Y.P. Pang, Zinc's exclusive tetrahedral coordination governed by its electronic structure, *Mol. Model. Annual.* 5 (7) (1999) 134–140.
- [34] N.J. Rose, R.S. Drago, Molecular addition compounds of iodine. I. An absolute method for the spectroscopic determination of equilibrium constants, *J. Am. Chem. Soc.* 81 (23) (1959) 6138–6141.
- [35] J.M. Mir, M.W. Khan, K. Diwan, A novel tetrahedral silver complex of (z)-o-methyl-s-hydrogen tosylcarbonimidothioate: DFT supported crystallographic and spectroscopic study, *J. Indian Chem. Soc.* 99 (8) (2022), 100626.
- [36] M. Govindarajan, M. Karabacak, Spectroscopic properties, NLO, HOMO–LUMO and NBO analysis of 2, 5-Lutidine, *Spectrochim. Acta, Part A* 96 (2012) 421–435.
- [37] M. Benavente, S. Arias, L. Moreno, J. Martínez, Production of glucosamine hydrochloride from crustacean shell, *J. Pharm. Pharmacol.* 3 (1) (2015) 20–26.
- [38] F.A. Al Sagheer, M.A. Al-Sughayer, S. Muslim, M.Z. Elsabee, Extraction and characterization of chitin and chitosan from marine sources in Arabian Gulf, *Carbohydr. Polym.* 77 (2) (2009) 410–419.
- [39] G. Giugliarelli, S. Cannistraro, Simulation of EPR spectra of Cu²⁺ complexes with statistical distribution of the g-factor and hyperfine splitting, *Chem. Phys.* 98 (1) (1985) 115–122.
- [40] N. Singh, K.K. Shukla, R.N. Patel, U.K. Chauhan, R. Shrivastava, ESR, magnetic, optical and biological (SOD and antimicrobial) studies of imidazole bridged CuII–ZnII and CuII–NiII complexes with tris (2-amino ethyl) amine as capping ligand: a plausible model for superoxide dismutase, *Spectrochim. Acta, Part A* 59 (13) (2003) 3111–3122.
- [41] S.I. Liochev, I. Fridovich, Copper- and zinc-containing superoxide dismutase can act as a superoxide reductase and a superoxide oxidase, *J. Biol. Chem.* 275 (49) (2000) 38482–38485.
- [42] T.H. Wang, L.T. Wang, W.L. Huang, L.Y. Huang, A DFT study on structures, frontier molecular orbitals and UV–vis spectra of RuX (PPh₃)(NHPh₂) L (X= Tp and Cp; L= Cl and N3), *Spectrochim. Acta, Part A* 121 (2014) 650–656.
- [43] A. Zianna, S. Vecchio, M. Gdaniec, A. Czapik, A. Hatzidimitriou, M. Lalia-Kantouri, Synthesis, thermal analysis, and spectroscopic and structural characterizations of zinc (II) complexes with salicylaldehydes, *J. Therm. Anal. Calorim.* 112 (1) (2013) 455–464.
- [44] J.R. Allan, W.C. Geddes, C.S. Hindle, A.E. Orr, Thermal analysis studies on pyridine carboxylic acid complexes of zinc (II), *Thermochim. Acta* 153 (1989) 249–256.
- [45] J. Jayabharathi, V. Thanikachalam, M.V. Perumal, Studies on interaction between an imidazole derivative and bovine serum by spectral methods, *Spectrochim. Acta, Part A* 95 (2012) 622–626.
- [46] J.M. Mir, R.C. Maurya, Experimental and theoretical insights of a novel molybdenum (0) nicotine complex containing CN and NO as co-ligands, *J. Chin. Adv. Materials Soc.* 6 (4) (2018) 620–639.
- [47] R.C. Maurya, P.K. Vishwakarma, J.M. Mir, D.K. Rajak, Oxidoperoxomolybdenum (VI) complexes involving 4-formyl-3-methyl-1-phenyl-2-pyrazoline-5-one and some β -diketoenolates, *J. Therm. Anal. Calorim.* 1 (124) (2016) 57–70.
- [48] A. Yadav, S. Mohite, Anticancer activity and In-Silico ADMET analysis of malvastrum coromandelianum, *Int. J. Pharma Sci. Res.* 11 (5) (2020) 71–73.
- [49] S.A. Majid, J.M. Mir, M.A. Bhat, A.H. Shalla, A. Pandey, T.B. Hadda, M. H. Abdellattif, A pair of carbazate derivatives as novel Schiff base ligands: DFT and POM theory supported spectroscopic and biological evaluation, *J. Biomol. Struct. Dyn.* (2022) 1–7, <https://doi.org/10.1080/07391102.2022.2090437>.